

Double Exchange in Electron Doped $\text{Ca}_{1-x}\text{Y}_x\text{MnO}_3$ Manganites

H. Aliaga, M. T. Causa, H. Salva, M. Tovar, A. Butera and B. Alascio.
Centro Atómico Bariloche and Instituto Balseiro
Comisión Nacional de Energía Atómica and Universidad Nacional de Cuyo.
8400 San Carlos de Bariloche, Argentina.

D. Vega, G. Polla, G. Leyva, and P. König
Centro Atómico Constituyentes.
Comisión Nacional de Energía Atómica
1650 San Martín, Buenos Aires, Argentina.
(December 2, 2024)

We have studied magnetic and electric transport properties in the electron doped $\text{Y}_x\text{Ca}_{1-x}\text{MnO}_3$ manganite in the region $0 \leq x \leq 0.25$. We found an anomalous behavior in the temperature dependence of the susceptibility for low doped samples. With a simple model where antiferromagnetic (AF) superexchange and ferromagnetic double exchange (DE) interactions compete, we reproduce susceptibility vs. temperature measurements. From the fitting parameters, we have found that DE interaction is about twice as large than the AF interaction. We conclude that the competition between DE and AF are the main driving forces that explain the magnetic and electrical transport properties found in low Y-doped manganites.

PACS numbers: 75.30.Vn, 75.10.-b, 75.40.Mg

I. INTRODUCTION

The existence of magnetoresistance (MR) in Mn oxides with perovskite structure was discovered at the very early stage of the study of the transition metal oxides¹. The interest in these oxides has revived recently due to the discovery of very large MR ($\sim 10^6\%$) which led to call this phenomenon as colossal magnetoresistance (CMR). At the same time a magnetic field induced insulator-metal and structural transition² was also discovered. Most studies were devoted to the perovskite compounds $\text{R}_x\text{A}_{1-x}\text{MnO}_3$ (R=trivalent rare earth and A=divalent alkaline earth) producing $x \text{ Mn}^{3+}$ and $(1-x) \text{ Mn}^{4+}$ ions, respectively. Ferromagnetic (FM) double-exchange (DE) interaction between localized t_{2g} Mn electron configuration, mediated by itinerant spin-polarized e_g electrons, is in the base of CMR. The concentration x is not the only parameter to be taken into account in CMR materials. Chemical parameters such as the average R-A cationic radius and the cationic size mismatch quantified by the variance σ^2 of the ionic radii^{3,4} are also relevant. The phase diagrams for $\text{R}_x\text{A}_{1-x}\text{MnO}_3$ families were found to be non-symmetric and hole or electron doping cause disimilar effects. Theoretical studies⁵ suggested at least three possible scenarios to understand the low electron doping region: i) Canting of the magnetic structure. ii) Phase separation into ferromagnetic and antiferromagnetic phases and charge separation. iii) Ferromagnetic polarons. Therefore, experiments on families of compounds, covering different ranges of physical and chemical parameters can be used to clarify this issue. In this paper we study structural, transport and magnetic properties of $\text{Ca}_{1-x}\text{Y}_x\text{MnO}_3$. Trivalent Y is one of the smallest ions synthesizing in the perovskite

structure. For $x < 0.8$ an orthorhombic phase has been obtained⁶. Magnetoresistance effects were reported⁷ for $0.05 \leq x \leq 0.15$, indicating the presence of DE interaction. The non magnetic character of Y ions makes the series $\text{Ca}_{1-x}\text{Y}_x\text{MnO}_3$ an excellent system to study the evolution of the magnetism of Mn ions, without interference from other magnetic species. This is specially important in the paramagnetic regime. We present here magnetic measurements in the region $0 \leq x \leq 0.25$ and compare with the resistivity results of Ref. 7. We analyse these measurements in the PM and ordered phases to show that they can be understood in terms of small magnetic polaron⁸ arising from the DE mechanism between Mn^{4+} and Mn^{3+} .

II. EXPERIMENTAL

Ceramic polycrystalline samples of $\text{Ca}_{1-x}\text{Y}_x\text{MnO}_3$ were prepared by solid state reaction methods^{6,7}. Room temperature x-rays diffractograms show that CaMnO_3 crystallizes in an orthorhombic $Pnma$ cell with parameters $a=5.284(5)\text{\AA}$, $b=7.453(5)\text{\AA}$, and $c=5.266(5)\text{\AA}$. For $x \leq 0.25$ single phase material was obtained. Electrical resistivity was measured with the 4-probe method using a current source of $10-100\mu\text{A}$. The dc-magnetization M was measured with a SQUID magnetometer between 5K and 300K and $H \leq 50\text{kOe}$ and with a Faraday Balance magnetometer between 300K and 1000K with $H \leq 10\text{kOe}$.

III. RESULTS

In Fig. 1 we show H/M vs. T measured for the samples $x=0, 0.05, 0.07,$ and 0.10 . In all cases M is a linear function of H for $T \geq 140\text{K}$. A Van Vleck contribution is expected for Mn^{4+} ions⁹. In our measurements this contribution was subtracted in the paramagnetic phase, proportionally to $(1-x)$.

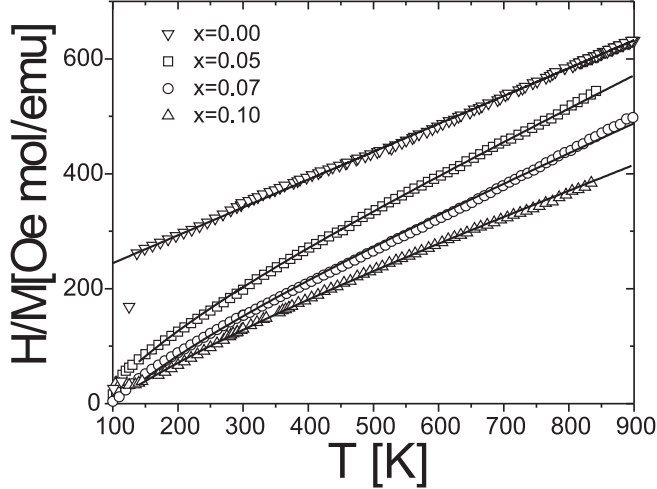


FIG. 1. Measured $\chi^{-1}(T)$ curves (symbols) with $H=10\text{kOe}$ and calculated (lines) for the samples $x=0, 0.05, 0.07$ and 0.10 . Notice the deviation from the Curie-Weiss law below $\simeq 450\text{K}$.

The CaMnO_3 data were fitted with a Curie Weiss law, $\chi = C/(T - \Theta)$, where C is the Curie constant and Θ is the Curie-Weiss temperature, obtaining $C = (1.95 \pm 0.05)$ emu K/mol (near the expected Mn^{4+} value 1.875) and $\Theta \approx -400\text{K}$. This value points to a strong antiferromagnetic (AF) superexchange interaction between Mn^{4+} ions. In this case M remains linear with H down to T_N . Using neutron diffraction, Wollan and Kohler¹⁰ found G-type AF ordering below $T_N \sim 123\text{K}$. The ratio $\Theta/T_N > 3$ is an indication of the importance of second neighbors interaction in the perovskite structure⁹. Further magnetic measurements have shown the existence of a weak ferromagnetic moment¹¹ below T_N of $\sim 0.03\mu_B/\text{Mn}$ ion.

For the samples $x > 0$, H/M deviates substantially from the Curie-Weiss law for $T \lesssim 450\text{K}$. In Fig. 2(a) it is shown the dependence of Θ with the doping x , as obtained from high T fits. Small Y doping causes large changes in the Θ values, indicating an evolution from a strong AF for $x=0$ ($\Theta \approx -400\text{K}$) to a FM one for $x \approx 0.10$ ($\Theta \approx +80\text{K}$).

In Fig. 3 we show M vs. T curves measured with $H = 5\text{kOe}$, for selected samples. Below $T \sim 125\text{K}$ a FM component that increases with x up to $x=0.10$ was measured. A magnetic transition temperature, T_{mo} , was defined as the temperature with maximum slope of $M(T)$. A detailed dependence of T_{mo} vs. x is shown in Fig. 2(b).

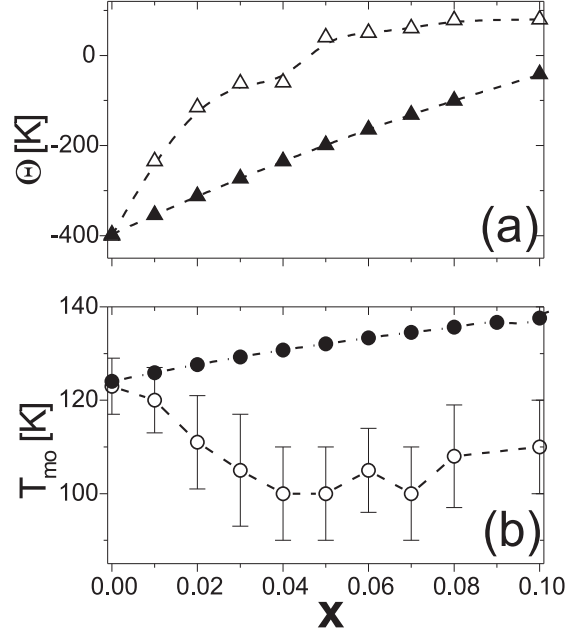


FIG. 2. (a) Measured (open) and calculated (solid) Curie-Weiss temperatures vs. x . Small Y doping cause an evolution from a strong AF state for low values of x to a FM one for x values greater than 0.06 . (b) Measured (open) and calculated (solid) magnetic ordering temperature vs. x .

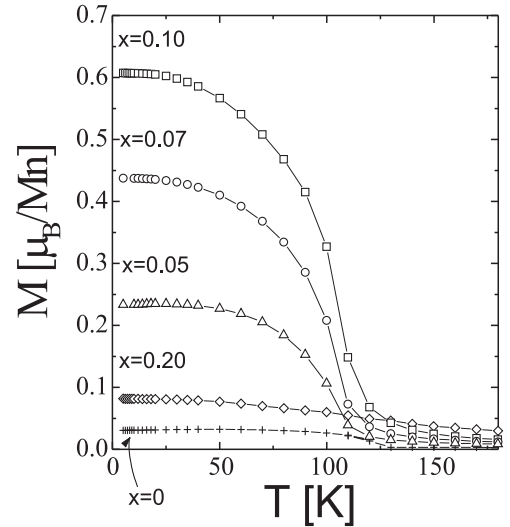


FIG. 3. M vs. T curves with $H=5\text{kOe}$. Lines are guides to the eye.

In Fig. 4 we show M vs. H at $T = 5\text{K}$. For $|H| \gtrsim 30\text{kOe}$, $M(H)$ can be approximated by: $M = M_0 + \chi_{AF} H$, where M_0 is the ferromagnetic contribution to M , and χ_{AF} is the high field differential susceptibility, which is almost independent of temperature well below T_{mo} . In the case of $x=0.1$, χ_{AF} shows a maximum around T_{mo} resembling the behaviour of an antiferromagnet. For $|H| \lesssim 10\text{kOe}$, $M(H)$ varies rapidly and reaches,

for $H = 0$, a small remanent magnetization (low compared with that of a typical FM), almost independent of x . In Fig. 5(a) we plot M_0 vs. x . Notice that M_0 is in all cases, much smaller than the expected value for full FM alignment ($M_S \sim 3\mu_B/\text{Mn ion}$). In the region $0 \leq x \leq 0.03$, $M_0(x)$ increases almost linearly, with an initial slope of $\sim 0.85\mu_B/\text{Mn ion}$. For $x \gtrsim 0.03$, M_0 increases more rapidly and reaches a maximum ratio $M_0/x \approx 7.1\mu_B/\text{Mn ion}$ for $x \sim 0.07-0.1$. For $x > 0.15$, M_0 decreases sharply. In Refs. 12-14, a similar behaviour was observed for other electron doped manganites; where Ca was substituted with different rare earths.

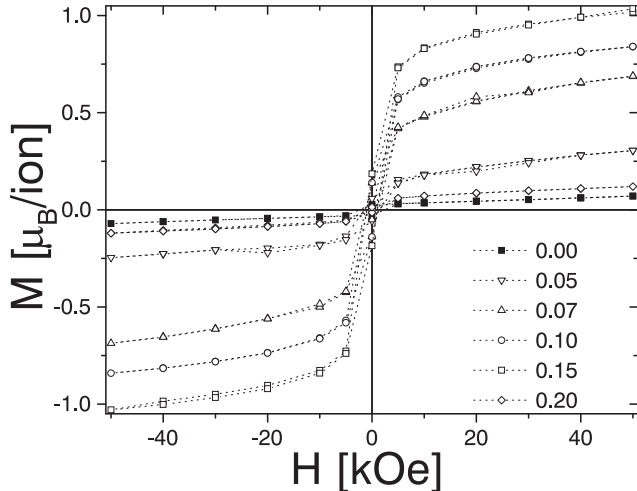


FIG. 4. M vs. H curves at 5K. Full alignment ($M_0 \sim 3\mu_B$) is not reached in any case. Dotted lines are guides to the eye.

In Fig. 5(b) we present the dependence of the electric resistivity $\rho(100\text{K})$ extracted from Ref. 7. The resistivity decreases 5 orders of magnitude between $x=0$ and $x=0.05$, remains almost constant for $0.05 \leq x \leq 0.15$, and then increases again for $0.15 \leq x \leq 0.25$. Comparing Figs. 5(a) and 5(b) in the range $0 \leq x \leq 0.15$, we see that the greater the concentration of carriers, the greater the conductivity and the magnetic moment. These results are in qualitative agreement¹⁵ with the DE mechanism. In the region $0.15 \leq x \leq 0.25$ the resistivity increases and the magnetic moment decreases, the DE mechanism is broken, leading to a low magnetic moment-insulator state.

IV. DISCUSSIONS

When Y^{3+} substitutes for Ca^{2+} in CaMnO_3 , e_g electrons are introduced in the system. These electrons polarize the AF background⁸, forming magnetic polarons. In the dilute region $x \sim 0$, we expect that Jahn-Teller distortions surrounding each Mn^{3+} localize the e_g electrons, forming a combined lattice-magnetic polaron. In this regime each polaron carries an extra magnetic moment due to the added e_g electron ($S = 1/2$). Within this

model the large variation of M with H for $|H| \leq 10\text{kOe}$ at low temperatures is mainly due to the alignment of these small magnetic polarons and a linear dependence of M_0 with x is expected, with $M_0/x = 1\mu_B/\text{Mn ion}$ (see Fig. 5a). The resistivity drops sharply possibly due to some distortion of the AF background, allowing the excitation of the e_g electrons from the localized Jahn-Teller states to a narrow conduction band. In the region $0.02 \leq x \leq 0.05$ these polarons interact with each other, so the M_0 vs x curve displays concavity.

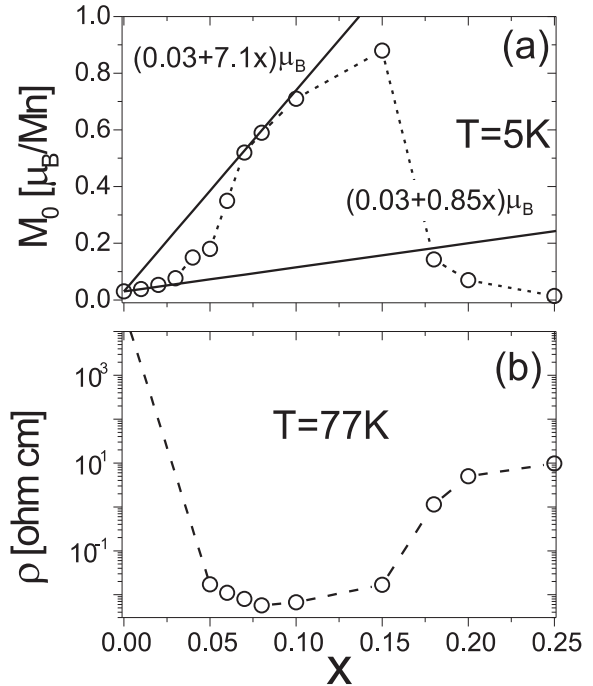


FIG. 5. (a) High Field extrapolated magnetization M_0 vs. x . Continuous straight lines indicates the initial and maximum slopes. (b) The zero field resistivity ρ vs. x , taken from Ref. 7. Notice the strong correlations between magnetism and resistivity. Dotted lines are guides to the eye.

For $x \geq 0.07$, we find $M_0/x \sim 7.1\mu_B/\text{Mn-ion}$, indicating that the polarons have a larger magnetic moment. The resistivity remains constant in this region and maximum magnetoresistance was measured⁷. We can interpret the results in the region $0.05 \leq x \leq 0.15$ with the following model: each Mn^{3+} that replaces a Mn^{4+} , couples ferromagnetically with the Mn^{4+} neighbors, after a spin flip process (see Fig. 6a). This ferromagnetic coupling is favoured by the kinetic energy gain due to the hopping of the e_g electron into the neighboring localized spins, forming a larger magnetic polaron, comprising the Mn^{3+} site and its nearest neighbors. This process is possible because of the G-type AF ordering. With zero applied field these Mn^{3+} spins, with a magnetic moment of $4\mu_B$, are oriented in random up and down directions in the lattice. When a magnetic field H is applied, the e_g electrons of the misaligned Mn^{3+} spins hop to a Mn^{4+} neighbor, which, in turn, has five

neighbors oriented in the direction of H . After two spin-flip processes (see Fig. 6b) a displaced polaron is aligned with the field and $M_0/x=7\mu_B/\text{Mn-ion}$ is expected. The linear increase of $M(H)$ observed at high fields is due, in our view, to the contribution of the AF background.

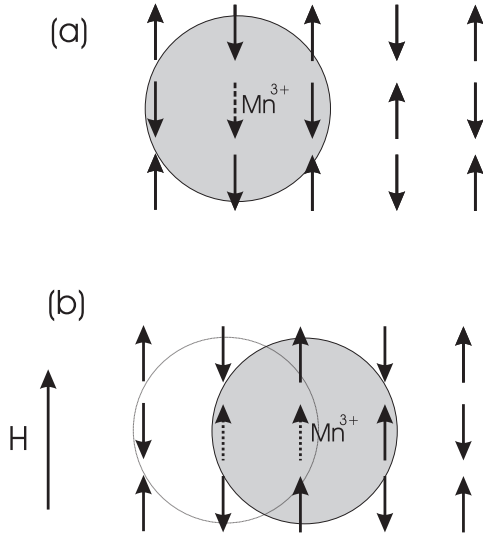


FIG. 6. (a) A Mn^{3+} that replaces a Mn^{4+} couples ferromagnetically with the Mn^{4+} neighbors, after a spin-flip process. (b) With an applied H the e_g electrons of the misaligned Mn^{3+} spins hop to a Mn^{4+} neighbor, with the $S = 3/2$ spin aligned with H after two spin-flip processes.

In the paramagnetic phase, the most peculiar feature observed is the deviation from the Curie-Weiss law, presenting a negative curvature of the $\chi^{-1}(T)$ curves (Fig. 1). In order to describe this behaviour, we consider the system as a mixture of Mn^{4+} and Mn^{3+} ions. Taking into account that the ordered state for $x=0$ is a G-type antiferromagnet we divide the system into two interpenetrated sublattices a and b , where Mn^{4+} and Mn^{3+} are randomly distributed with concentrations $(1-x)$ and x , respectively. We consider exchange interactions with first and second neighbors, between Mn^{4+} - Mn^{4+} , Mn^{3+} - Mn^{3+} and Mn^{4+} - Mn^{3+} pairs. The equations satisfied by the sublattice magnetizations in the mean field approximation are:

$$M_4^a T = C_4 [H + \gamma_{44}(1-x)M_4^b + \gamma'_{44}(1-x)M_4^a + \gamma_{43}xM_3^b + \gamma'_{43}xM_3^a] \quad (1)$$

$$M_4^b T = C_4 [H + \gamma_{44}(1-x)M_4^a + \gamma'_{44}(1-x)M_4^b + \gamma_{43}xM_3^a + \gamma'_{43}xM_3^b] \quad (2)$$

$$M_3^a T = C_3 [H + \gamma_{33}xM_3^b + \gamma'_{33}xM_3^a + \gamma_{43}(1-x)M_4^b + \gamma'_{43}(1-x)M_4^a] \quad (3)$$

$$M_3^b T = C_3 [H + \gamma_{33}xM_3^a + \gamma'_{33}xM_3^b + \gamma_{43}(1-x)M_4^a + \gamma'_{43}(1-x)M_4^b] \quad (4)$$

where subindexes 4 and 3 indicate Mn^{4+} and Mn^{3+} ions respectively, superindexes a y b correspond to the two sublattices, and γ_{ij} are the parameters describing the exchange coupling between M_i and M_j . Primed parameter indicate interaction with second neighbors. The total magnetization is given by:

$$M = \frac{1}{2}[(M_4^a + M_4^b)(1-x) + (M_3^a + M_3^b)x] \quad (5)$$

In the PM regime we take $M_4^a = M_4^b$ and $M_3^a = M_3^b$. Only three independent parameters ($\gamma_{44} + \gamma'_{44}$, $\gamma_{33} + \gamma'_{33}$ and $\gamma_{43} + \gamma'_{43}$) are necessary to fit the experimental curves in the paramagnetic zone, since first and second neighbors contribution cannot be separated. Best fits of the experimental data are shown in Fig. 1, where an excellent agreement is observed. For $x=0$ the solutions of Eqs. 1-4 correspond to a Curie-Weiss behaviour with a characteristic temperature $\Theta = C_4(\gamma_{44} + \gamma'_{44})$. From Fig. 1 we derived $\gamma_{44} + \gamma'_{44} = -204$ mol/emu. For $0 \leq x \leq 0.10$, the contribution to the total magnetization of the Mn^{3+} ions is small compared to the contribution of the Mn^{4+} species. For this reason we expect great indetermination in $(\gamma_{33} + \gamma'_{33})$, if left as a free parameter. Thus we have taken as an approximate fixe value, $(\gamma_{33} + \gamma'_{33}) = +73$ mol/emu, as obtained for the Mn^{3+} - Mn^{3+} interaction⁹ in the pseudo-cubic high temperature phase of LaMnO_3 . Therefore when fitting the data for $x > 0$, only $(\gamma_{43} + \gamma'_{43})$ is kept as an adjustable parameter. We obtained +361, +386 and +310 mol/emu for $x=0.05, 0.07$, and 0.10 , respectively. We have found that these results are rather insensitive to the value assumed for the Mn^{3+} - Mn^{3+} interaction, within the experimental uncertainty ($\sim 10\%$), if we take $-204 \text{ mol/emu} \lesssim (\gamma_{33} + \gamma'_{33}) \lesssim 73 \text{ mol/emu}$. The $(\gamma_{43} + \gamma'_{43})$ parameter is always positive and approximately two times larger than $\gamma_{44} + \gamma'_{44}$, denoting strong ferromagnetic coupling between Mn^{4+} and Mn^{3+} pairs. From now on, we take the average value $(\gamma_{43} + \gamma'_{43}) = +350$ mol/emu.

The behavior of the reciprocal susceptibility, $\chi^{-1}(T)$, is a hyperbola whose high temperature asymptote has a Curie-Weiss form, with $C = (1-x)C_4 + xC_3$ and

$$\Theta = C^{-1}[(1-x)^2 C_4^2 (\gamma_{44} + \gamma'_{44}) + 2(\gamma_{43} + \gamma'_{43})x(1-x)C_3 C_4 + x^2 C_3^2 (\gamma_{33} + \gamma'_{33})] \quad (6)$$

In Fig. 2(a) we compare measured and calculated Θ . Both curves show a similar behavior as a function of x , although the calculated Θ approaches a FM character less rapidly. Notice that the measured $\chi^{-1}(T)$ curves do not completely reach the asymptotic linear regime in the temperature range of the experiments. In order to analyze the magnetic ordering, Eqs. (1-4) must be solved for $H = 0$. The non-trivial solutions for M_i obtained for the highest temperature corresponds to the actual transition at T_{mo} . For $x = 0$, AF ordering is achieved for $T_{mo} = C_4(-\gamma_{44} + \gamma'_{44})$. The values $\gamma_{44} = -134$ mol/emu and $\gamma'_{44} = -71$ mol/emu are derived from the measured⁹ $T_N = 123$ K. The magnetic state found for small x preserves the

AF alignment between M_4^a and M_4^b . The Mn^{3+} ions are oriented FM with respect to their Mn^{4+} first neighbors in this dilute regime, irrespective of the value assumed for the Mn^{3+} - Mn^{3+} interaction. In this limit the ordering temperature is given by

$$T_{mo} \approx T_N(1-x) + (C_3C_4/T_N)(\gamma_{43} - \gamma'_{43})^2x(1-x) \quad (7)$$

where $T_N = T_{mo}$ ($x=0$). The first term reflects the dilution of the Mn^{4+} lattice and the second the combined effect of first and second neighbor Mn^{3+} - Mn^{4+} interactions. We have varied γ_{43} and γ'_{43} in order to reproduce the x dependence of T_{mo} , shown in Fig. 2(b). For $\gamma_{43} = 215$ mol/emu and $\gamma'_{43} = 135$ mol/emu, we found that T_{mo} increases continuously from $x=0$ to $x=0.1$, where a value of 137 K is reached, reproducing the experimental tendency for $x>0.04$. The initial decrease of T_{mo} cannot be included in this description with a unique set of parameters in Eq. (7).

V. CONCLUSIONS

We have measured structural, magnetic and transport properties as function of temperature and magnetic field in the manganites $Ca_{1-x}Y_xMnO_3$, for $0 \leq x \leq 0.25$. Despite of the small cationic size of Y, and the large cationic mismatch between Y and Ca, we have synthesized single phase material with orthorhombic structure. Strong correlation between magnetization and conductivity in the region $0 \leq x \leq 0.15$ was found, allowing to conclude that DE mechanism is present in this compound. The measurements in $Ca_{1-x}Y_xMnO_3$ show that the magnetic and electrical transport properties share a common behaviour with other $Ca_{1-x}A_xMnO_3$, with A=Lanthanides and Th, in spite of the important mismatch caused by the small size of Y^{3+} ions. This result confirms that among the three factors governing the CMR properties in hole doped perovskites: carrier density, average size and size mismatch, the electron concentration is predominant⁴ in electron doped materials. In the paramagnetic region we have found that $\chi^{-1}(T)$ curves deviate substantially from the Curie-Weiss law, showing strong ferromagnetic (DE) correlations, competing with the AF interaction of the background material. We have also have found that the high field extrapolated magnetization increases with the electron concentration, reaching $M_0 \approx 1\mu_B$ for $x \sim 0.15$, that is far from the value expected for full FM alignment ($M_0 \approx 3\mu_B$). We have interpreted these results in terms of magnetic polarons, and we propose that the low field response of M vs. H is due to the displacement of the e_g electrons from one magnetic sublattice to the other, causing the alignment of the polaron with the external field (Fig. 6). We discuss our results through a mean field model where FM and AF interactions between Mn^{3+} and Mn^{4+} spins compete. Form the fits of $\chi^{-1}(T)$ and using the measured values of T_{mo} we obtained values for the parameters of the model, that indicate that the

FM interactions are about twice the intensity of the AF interaction.

Acknowledgements : We acknowledge partial support from ANPCYT (Argentina)-PICT 3-52-1027, and CONICET(Argentina)-PIP 4947/96. H. A. is CONICET (Argentina) PhD-fellow.

-
- ¹ C. W. Searle and S. T. Wang, Can. J. Phys. **47**, 2023 (1969).
 - ² Y. Tokura and Y. Tomioka, J. Mag. Mag. Mat. **200**, 1 (1999).
 - ³ L. M. Rodríguez-Martínez and J. P. Attfield, Phys. Rev B **54**, R15622 (1996).
 - ⁴ C. Martin, A. Maignan and M. Hervieu, B. Raveau, Phys Rev B **60**, 12191 (1999).
 - ⁵ E. Dagotto, S. Yunoki, A. L. Malvezzi, A. Moreo, J. Hu, S. Capponi, D. Poilblanc, N. Furukawa, Phys. Rev. B, **58**, 6414 (1998).
 - ⁶ D. Vega, G. Leyva, G. Polla, P. König, H. Lanza, A. Esteban, H. Aliaga, M. T. Causa, M. Tovar and B. Alascio, J. Solid State Chem (in press).
 - ⁷ H. Aliaga, M. T. Causa, B. Alascio, H. Salva, M. Tovar, D. Vega, G. Polla, G. Leyva and P. König, J. Mag. Mag. Mat.(in press).
 - ⁸ C. D. Batista, J. Eroles, M. Avignon and B. Alascio, Phys. Rev. B **58**, R14689 (1998).
 - ⁹ D. L. Huber, A. Alejandro, A. Caneiro, M. T. Causa, F. Prado, M. Tovar and S. B. Oseroff, Phys. Rev. B **60**, 12155 (1999).
 - ¹⁰ E. O. Wollan and W. C. Kohler, Phys. Rev. **100**, 545 (1955).
 - ¹¹ G. H. Jonker, Physica **22**, 707 (1956); V. M. Yudin, A. I. Gavrilishina, M. V. Artemeva and M. F. Bryshina, Sov. Phys. Solid State **7**, 8 (1966); J. Briatico, B. Alascio, R. Allub, A. Butera, A. Caneiro, M. T. Causa and M. Tovar, Phys. Rev. B **53**, 14020 (1996).
 - ¹² A. Maignan, C. Martin, F. Damay and B. Raveau, Chem. Mater. **10**, 950 (1998); C. Martin, A. Maignan, F. Damay, M. Flervieu and B. Raveau, J. Solid State Chem. **134**, 198 (1997).
 - ¹³ I. O. Troyanchuk, H. Szymczak and A. Nabialek, J. Solid State Chem. **131**, 144 (1997).
 - ¹⁴ J. J. Neumeier and J. L. Cohn. Phys. Rev. B, **61**, 21, 14319 (2000).
 - ¹⁵ C. Zener, Phys. Rev. **82**, 403 (1951); P. W. Anderson and H. Hasegawa, Phys. Rev. **100**, 675 (1955).